Applied Catalysis B: Environmental 88 (2009) 224–231

Contents lists available at ScienceDirect

Applied Catalysis B: Environmental

journal homepage: www.elsevier.com/locate/apcatb

Oxidation of nitric oxide to nitrogen dioxide over Ru catalysts

Landong Li, Lingling Qu, Jie Cheng, Jinjun Li, Zhengping Hao *

Research Center for Eco-Environmental Sciences, Chinese Academy of Sciences, Shuangqing Road 18#, Haidian Dist., Beijing 100085, PR China

ARTICLE INFO

Article history:
Received 28 August 2008
Received in revised form 22 September 2008
Accepted 26 September 2008
Available online 9 October 2008

Keywords:
NO oxidation
Ru catalysts
TiO_2
TPR

ABSTRACT

A series of TiO_2 supported catalysts were prepared by impregnation method in a rotary evaporator and evaluated for the oxidation of NO to NO_2. Among all catalysts studied, Ru/TiO_2 catalyst exhibited the best activity and a maximal NO conversion of *c.a.* 94% could be achieved at *c.a.* 275 °C at a high GHSV of 180,000 h^{-1}. For ruthenium catalysts, the effects of supports, ruthenium loadings, pretreatment conditions and experiment conditions (feed gas composition, GHSV) on NO oxidation to NO_2 were investigated in detail. The ruthenium catalysts were characterized by means of X-ray diffraction (XRD), CO pulse chemisorption, transmission electron microscopy (TEM) and temperature-programmed reduction (TPR) techniques. The active ruthenium species for NO oxidation were discussed based on the catalytic and characterization results. Moreover, the reaction mechanism for NO oxidation over Ru/TiO_2 catalyst was studied by means of *in situ* diffuse reflectance Fourier transform infrared spectroscopy (DRIFTS).

1. Introduction

Nitrogen oxides (NO*x*), from stationary and transportation sources, are major air pollutants that greatly contribute to the formation of photochemical smog and acid rain. The removal of NO*x* is always a hot topic forever in the field of environmental catalysis and various techniques have been proposed for the abatement of NO*x* from anthropogenic sources. For example, selective catalytic reduction (SCR) and NO*x* storage-reduction (NSR) are two major techniques for NO*x* abatement in excess oxygen. In the research of SCR and NSR, it is well established that the oxidation of NO to NO_2 is a very important step for the whole reaction. For NSR, NO is first oxidized to NO_2 and then stored on the basic component of catalyst as nitrates [1]. For HC-SCR, NO is oxidized to NO_2, which subsequently reacts with hydrocarbon to give out N_2 [2]. In recent years, the so-called "fast" SCR reaction ($4NH_3 + 2NO + 2NO_2 \rightarrow 4N_2 + 6H_2O$), in contrast to standard ammonia SCR reaction ($4NH_3 + 4NO + O_2 \rightarrow 4N_2 + 6H_2O$), is receiving more and more attention [3–9]. The reaction between equimolar NO–NO_2 and NH_3 is *c.a.* 10 times faster than the reaction between NO and NH_3 at low temperatures (200–300 °C) [10]. Therefore, the fast SCR reaction is considered as a feasible means to boosting the denitrification efficiency at lower temperatures as well as to reducing the catalyst costs of SCR system. It is also noted that most nitrogen oxides from exhaust emissions exist in the form of NO (>90%), so that an upstream pre-oxidation catalyst converting NO to NO_2 is absolutely necessary to realize fast SCR reaction.

In the research of catalysts for NO oxidation, much effort has been focused on supported platinum materials. Pt/SiO_2 [11–13] and Pt/Al_2O_3 [13,14] were reported to be highly active for NO oxidation. The catalytic kinetics and the effects of preparation parameters on activities had been investigated in detail [11–14]. Although supported platinum catalysts show considerable activity for NO oxidation, the high cost of noble metal platinum materials restricts the application of supported Pt catalysts to a great extent. Moreover, the activity loss of supported platinum catalyst in strong oxidizing conditions remains a problem to be solved. Other catalysts, such as supported cobalt catalysts, are now being investigated as alternative catalysts for NO oxidation [15–18].

During the past decades, supported ruthenium materials have been extensively studied as catalysts for a number of reactions, *e.g.* organic synthesis [19], partial oxidation of hydrocarbons [20], Fischer–Tropsch synthesis [21] and ammonia synthesis [22]. Recently, ruthenium catalysts have been applied in the reaction of wet air oxidation of various pollutants [23–25] and complete oxidation of volatile organic compounds [26]. The good redox behaviors of ruthenium catalysts have been proved in these reactions, and supported ruthenium materials are thus expected to be good catalysts for other oxidation reactions. However, up to now, few researches have been focused on the application of ruthenium catalysts in the oxidation of nitric oxide to nitrogen dioxide.

In the present study, the activities of different transition metal catalysts for NO oxidation are investigated and supported ruthenium catalysts are found to be very active for the first time.

* Corresponding author. Tel.: +86 10 6292354; fax: +86 10 6292354.
E-mail address: zpinghao@rcees.ac.cn (Z. Hao).

0926-3373/$ – see front matter © 2008 Elsevier B.V. All rights reserved.
doi:10.1016/j.apcatb.2008.09.032

The effects of supports, ruthenium loadings, pretreatment of catalysts and reaction conditions (feed gas composition, GHSV) on NO oxidation are investigated in detail. More important, the active ruthenium species for NO oxidation are discussed based on the catalytic and characterization results.

2. Experimental

2.1. Catalysts preparation

The following oxides were selected as catalyst supports: SiO_2 (Sinopec), Al_2O_3 (Sinopec), ZrO_2 (Sinopec), TiO_2 (Degussa P25, 70% anatase, 30% rutile), TiO_2-Anatase (denoted as TiO_2-A, Fluka), TiO_2-Rutile (denoted as TiO_2-R, Degussa). Diffluent metal salts of analytical agent grade (NH_4VO_3, $CrCl_3$, $MnSO_4$, $FeCl_3$, $CoCl_2$, $NiCl_2$, $CuCl_2$, $PdCl_2$, $RhCl_3$, $RuCl_3$, H_2PtCl_6, $HAuCl_4$) were used as sources for supported materials without further purification.

The catalysts were prepared by impregnating the supports with aqueous solution of metal salt in a rotary evaporator at the constant temperature. In a typical preparation process of Ru/TiO_2, 20 mL $RuCl_3$ aqueous solution (Ru concentration: 1.0 mg/mL) was added to 1 g TiO_2 (P25) support. The impregnated sample was mixed well and then evaporated in a rotary evaporator at constant temperature of 80 °C. The as-prepared samples were carefully washed by distilled water, dried at 100 °C over night and then calcined at 450 °C in flowing air for 4 h. The Pt/TiO_2 sample was further reduced in 5%H_2/He at 450 °C for 1 h prior to catalytic test.

2.2. Catalyst characterization

The ruthenium contents in supported ruthenium catalysts were determined by ICP-AES using an Optima 2000 spectrometer. The surface areas of catalysts were analyzed by low temperature N_2 adsorption/desorption using a Quantachrome NOVA-1200 gas absorption analyzer and the specific surface areas were calculated using the BET equation.

The X-ray diffraction patterns of samples were recorded on a Rigaku powder diffractometer (D/MAX-RB) using Cu Kα radiation (λ = 0.15418 nm) at a scanning rate of 4°/min in 2θ = 5–80°.

The dispersion of ruthenium on various supports was determined by CO pulse adsorption on a chemisorption analyzer (Chemisorb 2720, Micromeritics). In a typical experiment, *c.a.* 100 mg sample in the quartz reactor was first reduced in 5%H_2/He at 450 °C for 1 h and pretreated in He at 450 °C for 1 h to remove H_2 adsorbed on the surface of samples. After cooling down to room temperature in flowing He, pulses of 5%CO/He were injected to the reactor one pulse per minute until no further changes in signal intensity of outlet CO. The dispersion of ruthenium was calculated assuming the equimolar adsorption of CO on ruthenium metal.

The temperature-programmed reduction experiments of samples were carried out on a chemisorption analyzer (Chemisorb 2720, Micromeritics) with 5 vol.% H_2/Ar at a heating rate of 10 °C/min from 50 to 600 °C. Prior to reduction, the sample (100 mg) was treated in He at 450 °C for 1 h.

Transmission electron microscopy images of samples were acquired on a JEOL 2010 transmission electron microscope at an acceleration voltage of 200 kV. A few drops of alcohol suspension containing the catalyst sample were placed on a carbon-coated copper grid, followed by evaporation at ambient temperature.

2.3. Catalytic oxidation of nitric oxide

The catalytic oxidation of NO was performed in a fixed-bed flow microreactor at atmospheric pressure. Typically, 0.15 g sample (sieve fraction, 0.25–0.5 mm) was placed in a quartz reactor (4 mm i.d.) and pretreated in 5%O_2/He (5%H_2/He for Pt/TiO_2 sample) at 450 °C for 1 h. After cooling to 150 °C in He, the reactant gas mixture (400 ppm NO, 10% O_2, He balance) was fed to the reactor. The total flow-rate of the gas mixture was kept at 450 mL min^{-1}, corresponding to a GHSV of 180,000 h^{-1}. The inlet and outlet gases were monitored on-line using a gas chromatograph (HP 6820 series, for N_2 and N_2O analysis) and a chemiluminescence NO*x* analyzer (Ecotech EC 9841, for NO and NO_2 analysis).

2.4. In situ DRIFT study of NO and NO–O_2 adsorption

In situ DRIFT studies were performed on the spectrometer (Bruker Tensor 27) with 128 scans at a resolution of 4 cm^{-1}. A self-supporting pellet (*c.a.* 50 mg) made of the catalyst sample was placed in the IR flow cell and the background spectrum was taken at desired temperatures in flowing He. For NO adsorption, 1% NO in He was fed to catalyst cell at room temperature and a series of time-dependent DRIFT spectra of NO adsorption were sequentially recorded. For NO–O_2 co-adsorption, the gas mixture (400 ppm NO, 10% O_2, balance He) was fed to the sample cell at a total flow-rate of 60 mL min^{-1} at 150 °C. After holding this temperature for 20 min, it was stepwise increased to the next designed temperature. The DRIFT spectra were recorded every 25 °C (from 150 to 350 °C) after 20 min of steady state reaction.

3. Results and discussion

3.1. NO oxidation activity over TiO_2 supported catalysts

The temperature dependence of steady-state NO oxidation over a series of TiO_2 supported catalysts is shown in Fig. 1. For reference, the thermodynamic equilibrium for NO–NO_2 under given conditions is also shown in the figure (in dashed). The main product for NO oxidation was NO_2, and the formation of other N-containing product (N_2O, N_2, etc.) could be neglected. The NO conversion to NO_2 over catalysts was kinetically limited at low temperatures and equilibrium-limited at higher temperatures. After reaching thermodynamic equilibrium, if possible, the NO conversion to NO_2 closely followed the thermodynamic equilibrium curve. Among TiO_2 supported transition metal oxides investigated, the best activity was obtained over Co/TiO_2 sample and the activity order was observed as $Co/TiO_2 > Mn/TiO_2 > V/TiO_2 > Cu/TiO_2 > Fe/TiO_2 > Cr/TiO_2 > Ni/TiO_2$. Among TiO_2 supported precious metal or metal oxides studied, Ru/TiO_2 showed the best activity, followed by Rh/TiO_2 and then Pd/TiO_2 and Au/TiO_2. The Pt/TiO_2 catalyst showed good activity at low temperatures (<225 °C), however its activity at high temperatures was observed to be lower than Rh/TiO_2. It should be mentioned that the Pt/TiO_2 was pre-reduced before reaction, considering that Pt metal was reported be more active than Pt oxides [11,14]. Ru/TiO_2 was the most active catalyst among TiO_2 supported catalysts for NO oxidation and a 50% NO conversion to NO_2 was achieved at *c.a.* 250 °C at a very high GHSV of 180,000 h^{-1}. The maximal NO conversion of *c.a.* 94% could be achieved at *c.a.* 275 °C.

The XRD patterns of TiO_2 supported catalysts studied are shown in Fig. 2. Typical diffraction peaks of TiO_2 support corresponding to anatase (JCPDS 21-1272) and rutile (JCPDS 21-1276) phase were observed, as marked in the XRD patterns. Besides, no diffraction peaks corresponding to the supported phases, neither in metal form nor in oxide form, could be observed. It is deduced that the supported phases are highly dispersed on TiO_2 support. The TEM image of Ru/TiO_2 catalyst is displayed in Fig. 3. It is seen that homogeneous nano-clusters with averages diameters of below 5 nm are evenly dispersed on the surface of TiO_2 support.

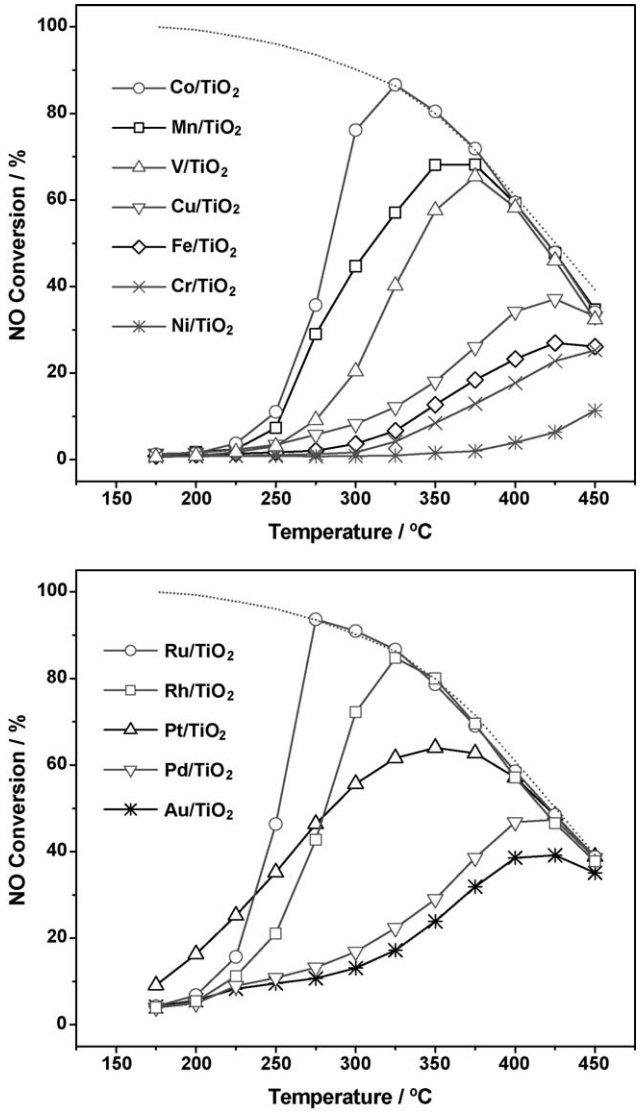

Fig. 1. Catalytic activities for NO oxidation on TiO_2 supported catalysts. Reaction conditions: 0.15 g catalyst, 400 ppm NO, 10% O_2 and the balance He, GHSV = 180,000 h^{-1}.

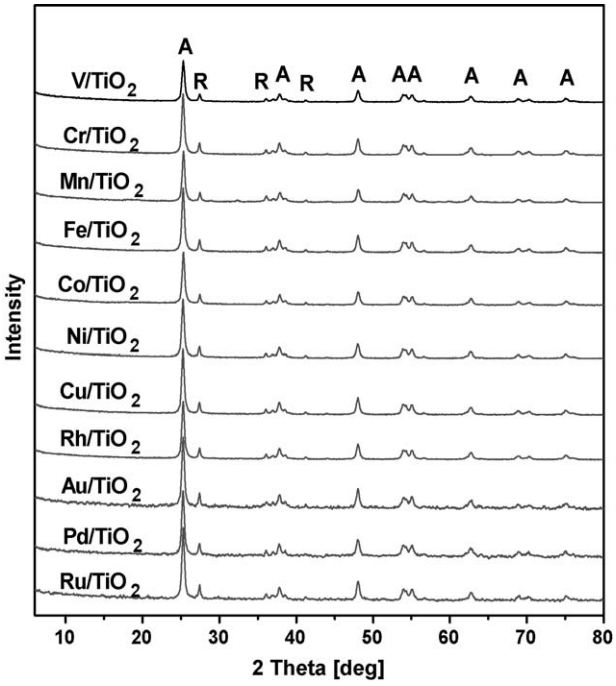

Fig. 2. XRD patterns of TiO_2 supported catalysts. R: rutile TiO_2; A: anatase TiO_2.

3.2. Effects of supports and Ru loadings on NO oxidation over Ru catalysts

The activities of Ru catalysts for NO oxidation are significantly dependent on the supports. The comparison of various supported Ru catalysts is shown in Fig. 4 and the activity order of these catalysts is observed as $Ru/TiO_2 > Ru/TiO_2$-R $> Ru/ZrO_2 > Ru/SiO_2 > Ru/Al_2O_3 > Ru/TiO_2$-A. Obviously, the BET surface areas of Ru catalysts do not play a decisive on their activities (Table 1). Ru/TiO_2-R sample with lowest surface area (21.5 m^2/g) exhibited quite high activity while Ru/Al_2O_3 with highest surface area (95.3 m^2/g) exhibited the very low activity. It is also seen that rutile phase TiO_2 appears to be much better support than anatase phase TiO_2. TiO_2 P25 with both anatase and rutile is the best support for Ru since Ru/TiO_2 exhibited the best activity among Ru catalysts studied.

The XRD patterns of supported Ru catalysts are shown in Fig. 5. In the XRD patterns of Ru/TiO_2, Ru/TiO_2-A, Ru/TiO_2-R, Ru/ZrO_2 and Ru/SiO_2, only diffraction peaks corresponding to supports are observed and no peaks ascribable to ruthenium species can be observed. While in the case of Ru/Al_2O_3, clear diffraction peaks ascribable to RuO_2 were observed besides the diffraction peaks corresponding to supports. The appearance of diffraction peaks ascribable to RuO_2 phase in the XRD patterns indicates the formation of bulk RuO_2 with high crystallinity.

The dispersion of Ru on different supports was analyzed by means of CO chemisorption and the data obtained are listed in Table 1. As expected, great difference in the dispersion of Ru is observed on different supports. The highest Ru dispersion of 70.5% is obtained in the case of Ru/TiO_2-R, while the lowest Ru dispersion of 21.8% is obtained in the case of Ru/Al_2O_3. The properties of supports play a decisive role on the dispersion of Ru species. The formation of bulk RuO_2 on supports undoubtedly results in the low dispersion of Ru, *e.g.* in the case of on Ru/Al_2O_3. Moreover, the

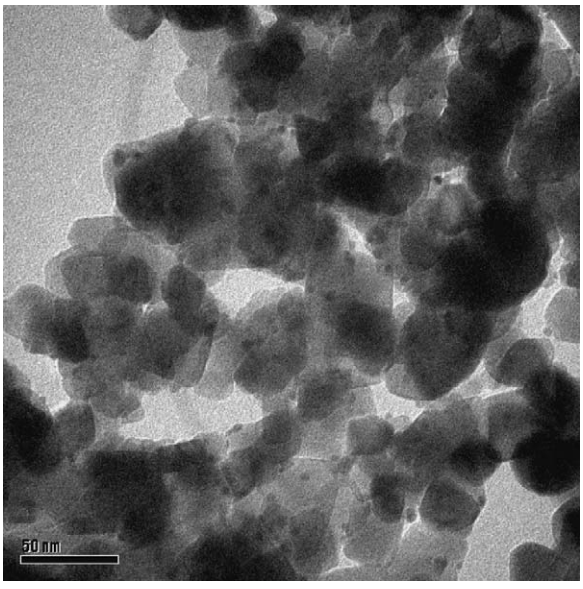

Fig. 3. TEM image of Ru/TiO_2 catalyst.

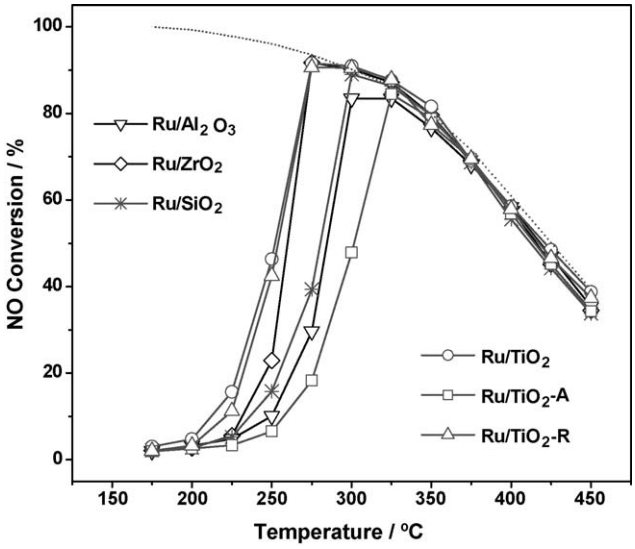

Fig. 4. Catalytic activities for NO oxidation on various supported Ru catalysts. Reaction conditions: 0.15 g catalyst, 400 ppm NO, 10% O_2 and the balance He, GHSV = 180,000 h^{-1}.

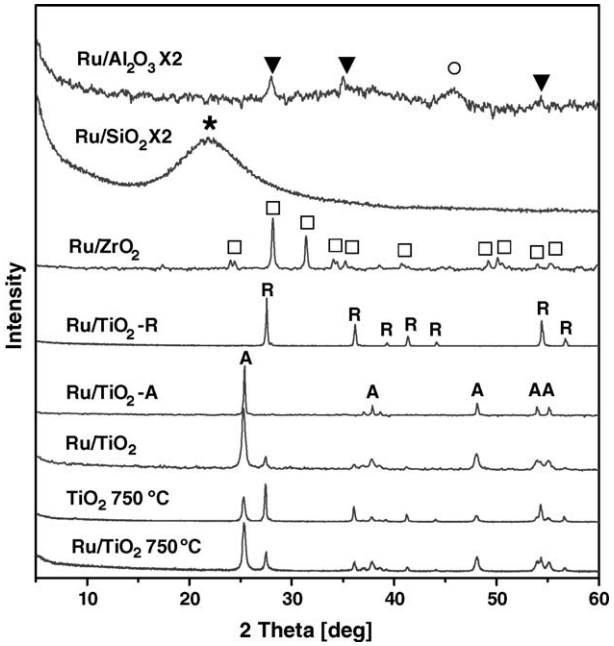

Fig. 5. XRD patterns of various supported Ru catalysts. R: rutile TiO_2; A: anatase TiO_2; (□) monoclinic ZrO_2; (*) amorphous SiO_2; (○) γ-Al_2O_3; (▼) RuO_2.

crystal phase of support might have essential effect on Ru dispersion. The Ru dispersion was the highest (70.5%) on rutile phase TiO_2 while the Ru dispersion was rather low (24.7%) on anatase phase TiO_2. It is seen that the dispersion of Ru species on support relates to the activity of Ru catalysts to some extent. Generally, higher dispersion of Ru species in Ru catalysts corresponds to higher NO oxidation activity. For example, Ru/Al_2O_3 with lowest Ru dispersion of 21.8% exhibited the very low NO oxidation activity. While Ru/TiO_2-R catalyst with highest Ru dispersion of 71.5% exhibited quite good NO oxidation activity. It is known that the dispersion of metal is greatly related to the Ru species formed on different support. So, it is proposed that the different Ru species formed on the supports may be responsible for the activity difference in Ru catalysts.

The different Ru species on supports are investigated by means of temperature-programmed reduction and the H_2-TPR profiles of Ru catalysts, together with reference amorphous RuO_2 sample, are shown in Fig. 6. Since the support materials were almost irreducible from 100 to 250 °C, the reduction peaks in this temperature range correspond to the reduction of different kinds of ruthenium oxides. Particularly, the reduction peaks at *c.a.* 180 and 230 °C are attributed to the reduction of crystallized RuO_2 to Ru^0, in well-dispersed form and bulk form, respectively [26,27]. The reduction peak at 125 °C in the low temperature range is attributed to the reduction of poorly crystallized or so-called amorphous bulk RuO_x. The reduction peak at higher temperature of 150 °C is attributed to the reduction of amorphous RuO_x with Ru–support interaction while reduction peak at the lower temperature of 105 °C is attributed to the reduction of highly dispersed amorphous RuO_x. The reduction peak at 75 °C in the TPR profile of reference amorphous RuO_2 sample should be attributed to the reduction of atomically dispersed Ru^{n+} [28]. As seen in Fig. 6, multiple H_2 reduction peaks are observed on Ru catalysts, indicating the formation of different kinds of ruthenium oxides. The TPR profiles are carefully deconvoluted and the amount of H_2 consumption of each reduction peak is summarized in Table 2. The total H_2 consumption indicated that most ruthenium oxides existed in the state of Ru^{4+}, *i.e.* RuO_2. By comparing the TPR data in Table 2 with the activity data in Fig. 4, we easily find that ruthenium oxides reducible at lower temperature exhibited higher activity for NO oxidation. As for Ru/TiO_2, Ru/TiO_2-R and Ru/ZrO_2, only amorphous ruthenium oxides reducible at low temperature were formed on supports, so high NO oxidation activity were observed on these catalysts. In the case of Ru/Al_2O_3, a large proportion of ruthenium species existed in the form of bulk RuO_2 that could be reduced at relative high temperature (XRD patterns in Fig. 5 and TPR profiles in Fig. 6), so Ru/Al_2O_3 exhibited the lowest activity.

Table 1
Physical properties of various supported ruthenium catalysts.

Catalyst	Ru loading (wt%)	Surface area (m^2/g)	CO uptake (μmol g^{-1})	Ru dispersion (%)
Ru/SiO_2	1.92	87.1	69.8	36.7
Ru/ZrO_2	1.95	75.9	89.8	45.6
Ru/Al_2O_3	1.88	95.3	41.4	21.8
Ru/TiO_2	1.96	49.2	135.6	68.5
Ru/TiO_2	3.87	51.8	219.9	57.4
Ru/TiO_2	0.95	52.7	67.1	71.3
Ru/TiO_2	0.48	54.5	34.6	72.8
Ru/TiO_2-R	1.91	21.5	136.1	70.5
Ru/TiO_2-A	1.95	23.4	48.6	24.7
Ru/TiO_2-750	1.39	17.3	14.7	10.5

The effect of Ru loading (0.5–4%) in Ru/TiO_2 on the activity of NO oxidation was studied and the results are shown in Fig. 7. As expected, Ru/TiO_2-4% exhibited the highest activity while Ru/TiO_2-0.5% exhibited the lowest activity. However, it is also found that Ru/TiO_2-4% only showed a little higher activity than Ru/TiO_2-2% despite that the Ru loading was doubled from 2% to 4%. In this work, Ru/TiO_2-2% was the most suitable catalyst for NO oxidation taking both the activity and the cost of catalyst into account. For a further understanding of the effect of Ru loading on the activity of catalyst, temperature-programmed reduction experiments were conducted to explore the ruthenium species formed on TiO_2 with different Ru loadings. The TPR profiles in Fig. 8 reveal that Ru mainly exists in the form of amorphous RuO_2 with Ru–support interaction in Ru/TiO_2-0.5% and Ru/TiO_2-1% (listed in Table 2). In the case of Ru/TiO_2-2%, more than 50% of Ru exists in the form of highly dispersed amorphous RuO_2 (reduction peak at 105 °C, in

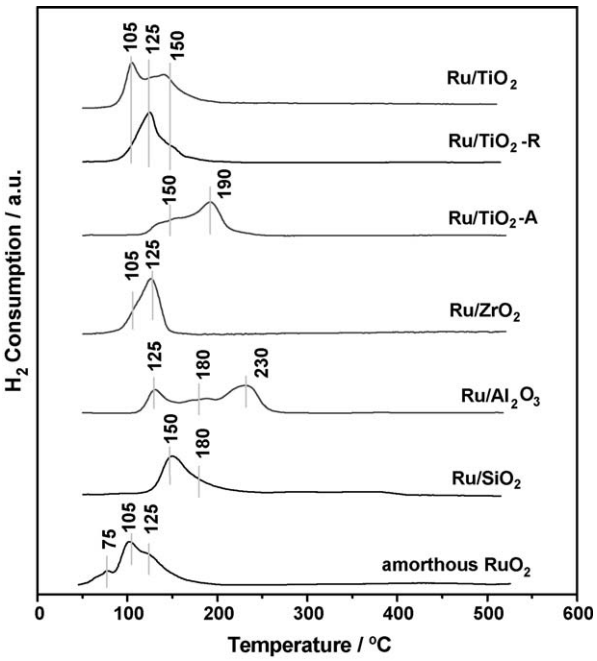

Fig. 6. H_2-TPR profiles of various supported Ru catalysts and amorphous RuO_2.

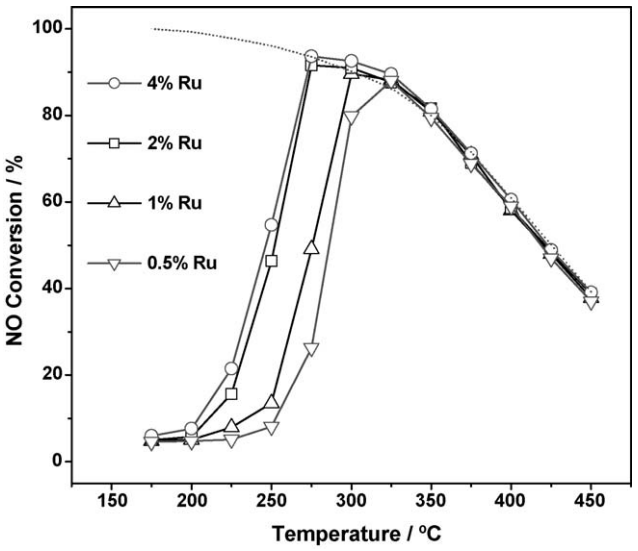

Fig. 7. Catalytic activities for NO oxidation on Ru/TiO_2 catalysts with different Ru loadings. Reaction conditions: 0.15 g catalyst, 400 ppm NO, 10% O_2 and the balance He, GHSV = 180,000 h^{-1}.

Table 2). This is the most active Ru species for NO oxidation, so Ru/TiO_2 exhibits quite higher activity than Ru/TiO_2-1%. The dispersion of Ru decreased from 68.5% to 57.4% with Ru loading increasing from 2% to 4%, and a large proportion of ruthenium species (>40%) existed in the form bulk amorphous RuO_2 in Ru/TiO_2-4% (Table 2). Since the amount of most active highly dispersed amorphous RuO_2 was similar in Ru/TiO_2-2% and Ru/TiO_2-4% (referred to the data of H_2 consumption in Table 2), Ru/TiO_2-4% only exhibited a little high activity for NO oxidation than Ru/TiO_2-2%.

3.3. Effects of experimental conditions on NO oxidation over Ru/TiO_2

We have investigated the effects of initial NO concentration in the gas stream on NO oxidation at a constant oxygen concentration of 10%. As shown in Fig. 9, the NO conversion to NO_2 decreases slightly with initial NO concentration increasing from 200 to 800 ppm. Particularly, the maximal NO conversion of *c.a.* 95% is observed at 275 °C with initial NO concentration of 200 ppm while the maximal NO conversion of *c.a.* 88% is observed at 300 °C with initial NO concentration of 800 ppm. Obviously, the oxidation of NO on Ru/TiO_2 catalyst is not an apparent first-order reaction under these reaction conditions.

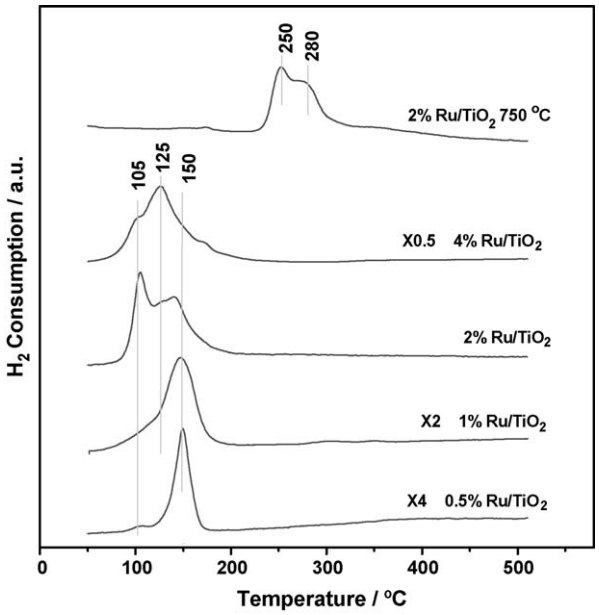

Fig. 8. H_2-TPR profiles of Ru/TiO_2 catalysts with different Ru loadings.

Table 2
H_2 consumption during TPR of supported ruthenium catalysts.

Catalyst	First reduction peak		Second reduction peak		Third reduction peak		Total H_2 (μmol g^{-1})[a]
	T (°C)	H_2 (μmol g^{-1})	T (°C)	H_2 (μmol g^{-1})	T (°C)	H_2 (μmol g^{-1})	
Ru/SiO_2	150	325.7	180	61.9	/	/	387.6
Ru/Al_2O_3	125	120.7	180	49.3	230	195.3	375.3
Ru/ZrO_2	105	67.9	125	309.7	/	/	377.6
Ru/TiO_2-A	150	69.8	190	317.5	/	/	387.3
Ru/TiO_2-R	105	67.1	125	287.6	150	41.5	396.2
Ru/TiO_2	105	205.8	125	73.5	150	110.8	390.1
Ru/TiO_2-0.5%	105	4.7	150	99.2	/	/	104.9
Ru/TiO_2-1%	105	5.2	125	24.7	150	150.8	180.7
Ru/TiO_2-4%	105	230.1	125	366.3	150	177.2	773.6
Ru/TiO_2-750	250	177.2	280	154.3	/	/	331.5

[a] Theoretical value = Ru loadings (wt%) × 19.8 mmol g^{-1} ($RuO_2 + 2H_2 \rightarrow Ru + 2H_2O$).

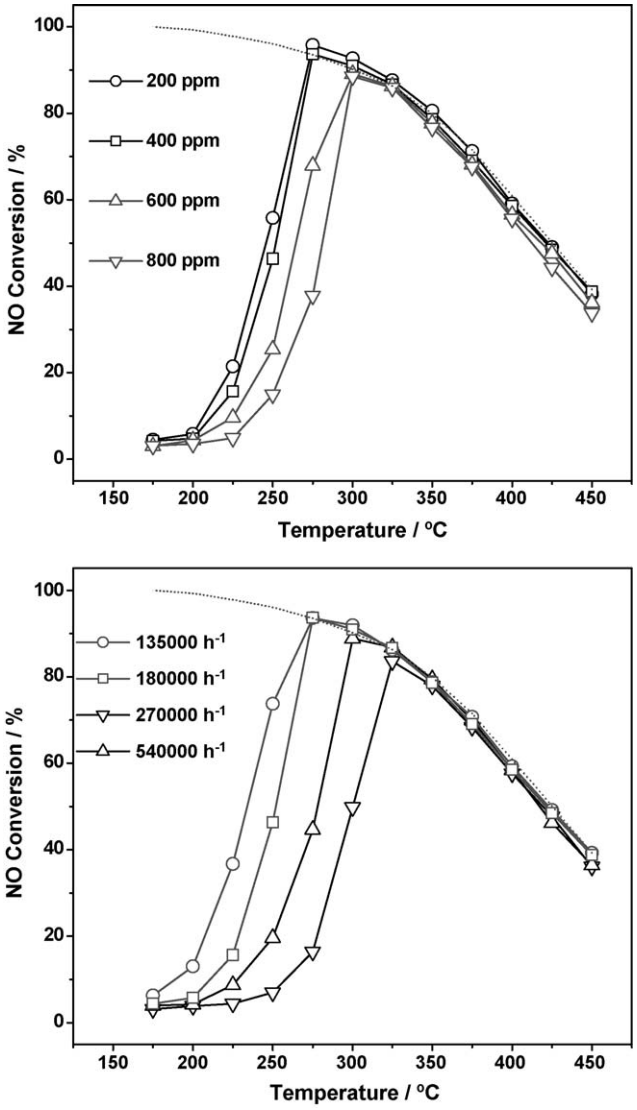

Fig. 9. Effects of initial NO concentration and GHSV on NO oxidation activity over Ru/TiO_2 catalyst.

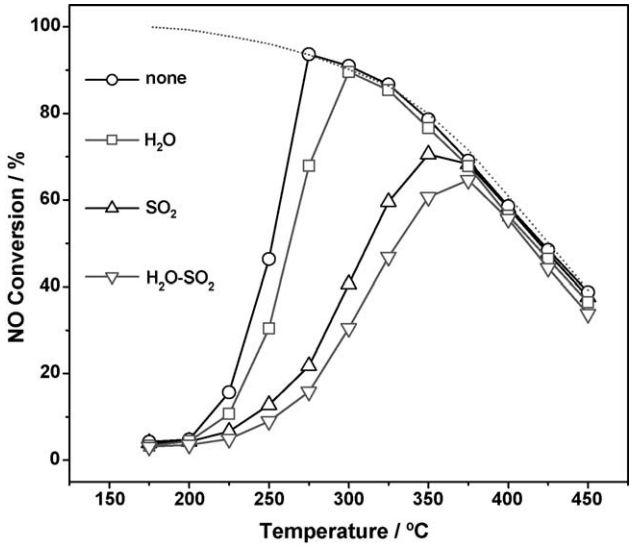

Fig. 10. Effects of SO_2 and H_2O in the stream on N_2O oxidation activity over Ru/TiO_2. Reaction conditions: 0.15 g catalyst, 400 ppm NO, 10% O_2 0 or 40 ppm SO_2, 0 or 2.5% H_2O and the balance He, GHSV = 180,000 h^{-1}.

The effects of GHSV on NO oxidation over Ru/TiO_2 are shown in Fig. 9. In this work, a very high GHSV of 180,000 h^{-1} was generally employed to reduce the amount of catalysts needed, so as to reduce the cost of catalysts. From Fig. 9, it is seen that NO conversion to NO_2 decreases with increasing GHSV from 135,000 to 540,000 h^{-1}. However, a maximal NO conversion of *c.a.* 84% could be obtained at 325 °C even at the highest GHSV of 540,000 h^{-1}. Also, it is possible to control the ratio of NO:NO_2 in the product, *e.g.* 1:1 for fast SCR, by changing the loadings of catalysts, *i.e.* adjusting the GHSV.

Since in a real NO emission source there are some SO_2 and water vapor in the stream, it is necessary to clarify their effects on NO oxidation. Water vapor in the reaction stream presents a negative impact on NO oxidation. As shown in Fig. 10, the presence of 2% H_2O reduces the NO conversion by 20–30% at 250–275 °C. The inhibition effect caused by water vapor is supposed to be due to process of following reaction [29]:

$$2NO_3^- + H_2O \rightarrow 2OH^- + NO + NO_2 + O_2$$

The addition of water vapor accelerated the decomposition of nitrate species on catalysts, which produced both NO and NO_2. As a result, NO conversion to NO_2 decreased slightly. The presence of 40 ppm SO_2 in the stream shows serious negative effect on N_2O decomposition. As seen in Fig. 10, the maximal NO conversion decreases from *c.a.* 94% to *c.a.* 69% and the temperature for maximal NO conversion increases from 275 to 350 °C with the addition of 40 ppm SO_2. Moreover, higher concentration of SO_2 may cause more serious deactivation of Ru/TiO_2 for NO oxidation (not shown in this work). SO_2 poisoning is known as the most serious problem for NO catalytic oxidation since catalysts preferred to convert SO_2 to SO_3 ($2SO_2 + O_2 \rightarrow 2SO_3$) instead of oxidation of NO. The formed SO_3 may not only occupy the active sites for NO oxidation but also cover the support materials by forming sulfates [11]. In this work, we selected SO_2-resistant TiO_2 as the support and tried to diminish the negative effect of SO_2 on NO oxidation. To our glad, Ru/TiO_2 appears to be relatively SO_2-resistant and NO oxidation activity over Ru/TiO_2 is sustainable in the presence of SO_2 at below 40 ppm level. When 2% water vapor and 40 ppm SO_2 coexist in the stream, the total inhibition effects are approximately accumulative (as seen in Fig. 10). On a whole, Ru/TiO_2 exhibits considerable activity for NO oxidation even in the present of water vapor and SO_2, *i.e.* the simulated condition of industrial NO emission sources.

3.4. Effects of catalysts pretreatment conditions on NO oxidation over Ru/TiO_2

The effects of catalysts pretreatment conditions on NO oxidation over Ru/TiO_2 are shown in Fig. 11. It is seen that the pre-oxidized sample (O_2, 450 °C) is much more active than the pre-reduced sample (H_2, 450 °C), indicating that Ru in oxides form (Ru^{4+}) was more active than Ru in metal form (Ru^0). It is also seen that thermal treatment in O_2 at higher temperatures results in the serious deactivation of Ru/TiO_2. For example, the maximal NO conversion decreased to *c.a.* 20% on sample treated at 750 °C. As is known, thermal treatment of TiO_2 leads to the transformation of anatase TiO_2 phase to rutile TiO_2 phase [30]. In the case of Ru/TiO_2, the transform of anatase to rutile caused by thermal treatment was suppressed to some extent by the addition of Ru, as indicated by XRD patterns in Fig. 5. Since rutile phase TiO_2 was better support than anatase TiO_2 (Section 3.2),

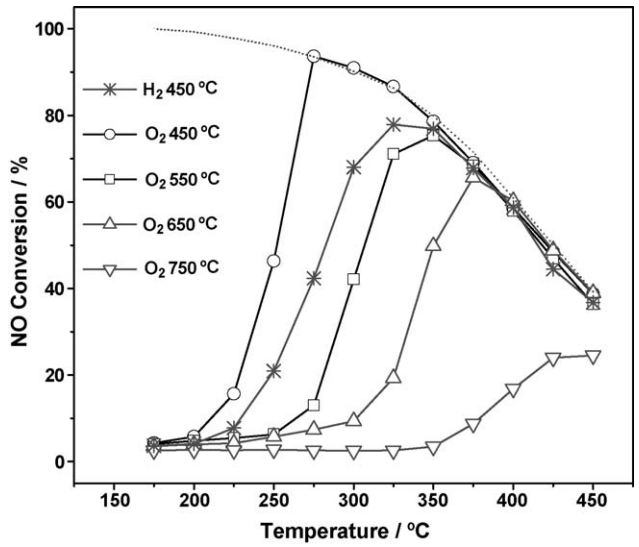

Fig. 11. Effects of pretreatment conditions on NO oxidation activity over Ru/TiO_2. Reaction conditions: 0.15 g catalyst, 400 ppm NO, 10% O_2 and the balance He, GHSV = 180,000 h^{-1}.

the transformation of anatase to rutile was not the main cause for the deactivation of Ru/TiO_2 by thermal treatment. The TPR profile of Ru/TiO_2-750 in Fig. 8 shows two reduction peaks at 250 and 280 °C, while the TPR profile of Ru/TiO_2 sample shows multiple reduction peaks at below 200 °C. The relay of Ru reduction indicated the strong interaction between Ru and TiO_2 support in Ru/TiO_2-750 sample, probably RuO_2 going into the matrixes of TiO_2. Meanwhile, the dispersion of Ru species also decreased from 68.5% to 10.5% after thermal treatment (Table 1). In our opinion, the formation of Ru species reducible at much higher temperatures was responsible for the lower activity of Ru/TiO_2-750. Except for the formation of Ru species reducible at higher temperatures, it was also found that some Ru left the catalyst after thermal treatment at 750 °C (Table 1), due to the formation of volatile RuO_4 at above 700 °C ($RuO_2 + O_2 \rightarrow RuO_4$) [31].

3.5. *In situ* DRIFT study of NO and NO–O_2 adsorption on Ru/TiO_2

Introduction of NO (1% in He) to Ru-TiO_2 sample at room temperature results in the appearance of several bands corresponding to various coordinated nitrites/nitrates, as displayed in Fig. 12. The bands at 1630 and 1320 cm^{-1} are assigned to the bridging nitrates at Ru–TiO_2 interface [32]. The band at 1440 cm^{-1} is assigned to mono-nitrite [33] while the band at 1350 cm^{-1} is assigned to chelating nitrites [34]. The intensity of IR bands corresponding to nitrates/nitrites increased with increasing adsorption time, and new IR band corresponding to mono-dentate nitrate [35] at 1500 cm^{-1} appeared after 9 min of NO adsorption. The surface species formed after NO adsorption on Ru/TiO_2 differ greatly from those on pure TiO_2 support reported by Hadjiivanov and Knozinger [36]. The modification of Ru to TiO_2 changes the oxidative activity and suppresses the formation of adsorbed nitrosyls (IR bands at 1966–1710 cm^{-1}). Since Ru/TiO_2 is able to oxidize NO to nitrite or nitrate species at room temperature, Ru/TiO_2 is expected as outstanding catalysts for NO oxidation at higher temperatures.

In situ DRIFT spectra obtained under reaction conditions over Ru/TiO_2 at different temperatures are shown in Fig. 12. At 150 °C, strong bands at 1630, 1600, 1500 and 1305 cm^{-1} as well as weak bands at 1875 and 1370 cm^{-1} have been observed. The bands at 1630 and 1600 cm^{-1} are assigned to different kinds of bridging nitrates [32,33], while the band at 1305 cm^{-1} is assigned to chelating nitrates [34]. The band at 1500 cm^{-1} is assigned to mono-dentate nitrate and the band at 1370 cm^{-1} is assigned to free nitrates [37]. The band at 1875 cm^{-1} is assigned to adsorbed NO species [38], most probably on RuO_2.

With increasing temperature, the intensity of IR bands associated with free nitrates increased gradually, while the intensities of IR bands associated with chelating nitrates and mono-dentate nitrate decreased gradually. Meanwhile, the intensities of IR bands associated with bridging nitrates remained

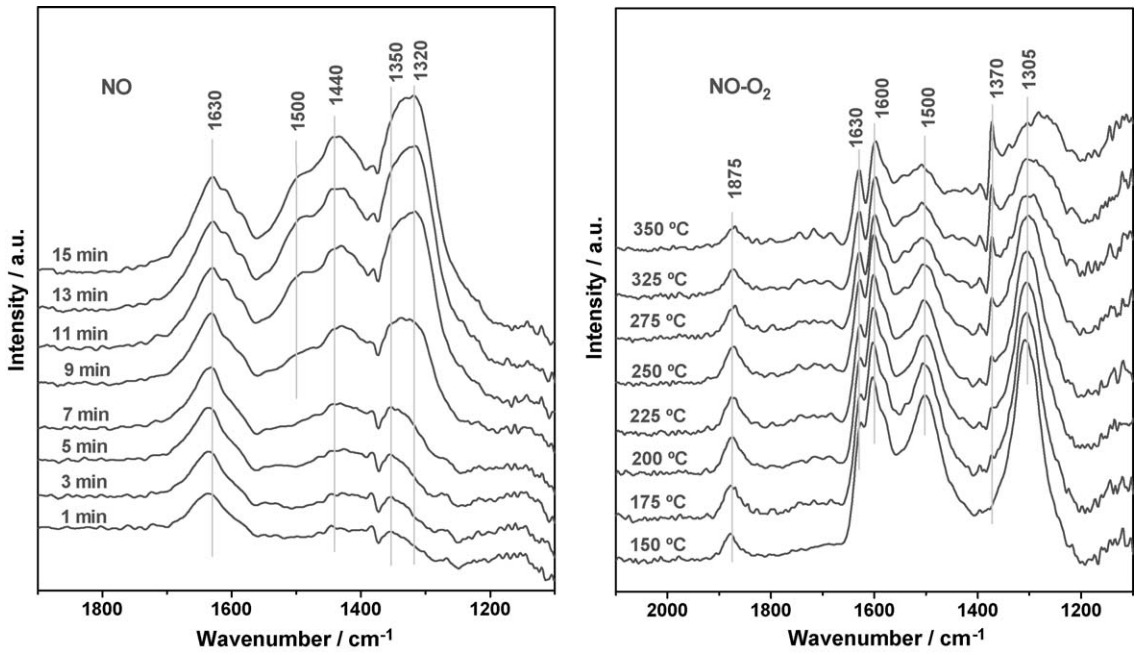

Fig. 12. Time-resolved DRIFT spectra of NO adsorption on Ru/TiO_2 at room temperature (left) and steady-state temperature-resolved DRIFT spectra of NO–O_2 co-adsorption on Ru/TiO_2 (right).

nearly unchanged. As for the IR band associated with adsorbed NO species, the band intensity increased first to a maximum (at 250 °C) and then began to decrease with increasing temperature. Based on the *in situ* DRIFT spectra, the NO oxidation mechanism on Ru/TiO_2 catalyst is proposed as following. In the first step, gaseous NO adsorbs on the surface of RuO_2 as $NO(g) + * \rightarrow -NO$ (*: active sites). The adsorbed NO species reacts with active oxygen to produce gaseous NO_2, with the release of the active sites ($-NO + O \rightarrow NO_2(g) + *$). In another possible way, the adsorbed NO can be further oxidized to various nitrates and migrate to the TiO_2 supports [39], known as $-NO + 2O \rightarrow -NO_3$. The bridging nitrates are relative stable nitrates at below 350 °C [33], so that they almost keep unchanged with increasing temperature, as indicated by Fig. 12. The chelating nitrates and mono-dentate nitrates are unstable species and they may decompose to give out NO_2 [40]. There are two possible pathways for the formation of gaseous product NO_2: the direct oxidation of adsorbed NO and the decomposition of surface nitrates. It is quite difficult to distinguish exactly which is the main pathway for NO_2 formation. In our experiments, the oxidation of NO to nitrates/nitrites takes place at room temperature (FTIR results), while the obvious oxidation of NO to gaseous NO_2 can only be observed at >175 °C (catalytic results). From this point of view, we prefer that NO_2 be originated by the decomposition of surface nitrates in the way as following: $4\text{-}NO_3 \rightarrow 4NO_2(g) + 1O_2(g) + 2\text{-}O$. At high temperatures of >275 °C, the catalytic decomposition NO_2 takes place accompanied by the oxidation of NO and as a result the NO conversion to NO_2 drops along the thermodynamic equilibrium.

4. Conclusion

The catalytic oxidation of NO over a series of TiO_2 supported catalysts prepared by impregnation method was studied. Ru/TiO_2 catalyst was found to be the most active among catalysts. The activities of Ru catalysts were related to support choice, Ru loadings, pretreatment conditions and reaction conditions. TiO_2 P25 with both anatase and rutile phase appeared to be the most suitable support of Ru and the optimal Ru loading was determined to be *c.a.* 2%. Increasing initial NO concentration and GHSV lowered the NO conversion to NO_2 over Ru/TiO_2 catalyst to some extent. Thermal treatment of catalyst at high temperature resulted in a severe deactivation of Ru/TiO_2 catalyst. The presence of H_2O and/or SO_2 in the reaction system showed obvious negative effects on NO oxidation over Ru/TiO_2. However, Ru/TiO_2 still exhibited considerable activity for NO oxidation even under the simulated condition of industrial NO emission sources. The formation of different kinds of RuO_2 species was observed on Ru catalysts and highly dispersed amorphous RuO_2 was proposed to be the most active Ru species.

Acknowledgements

This work was financially supported by the National Natural Science Foundation of China (20703057, 20725723).

References

[1] W.S. Epling, L.E. Campbell, A. Yezerets, N.W. Currier, J.E. Parks II., Catal. Rev. Sci. Eng. 46 (2004) 163–245.
[2] R. Burch, Catal. Rev. Sci. Eng. 46 (2004) 271–333.
[3] M. Koebel, M. Elsener, G. Madia, Ind. Eng. Chem. Res. 40 (2001) 52–59.
[4] M. Koebel, G. Madia, M. Elsener, Catal. Today 73 (2002) 239–247.
[5] I. Nova, C. Ciardelli, E. Tronconi, D. Chatterjee, B. Bandl-Konrad, Catal. Today 114 (2006) 3–12.
[6] M. Devadas, O. Kröcher, M. Elsener, A. Wokaun, N. Söger, M. Pfeifer, Y. Demel, L. Mussmann, Appl. Catal. B 67 (2006) 187–196.
[7] E. Tronconi, I. Nova, C. Ciardelli, D. Chatterjee, M. Weibel, J. Catal. 245 (2007) 1–10.
[8] C. Ciardelli, I. Nova, E. Tronconi, D. Chatterjee, B. Bandl-Konrad, M. Weibel, B. Krutzsch, Appl. Catal. B 70 (2007) 80–90.
[9] A. Grossale, I. Nova, E. Tronconi, D. Chatterjee, M. Weibel, J. Catal. 256 (2008) 312–322.
[10] A. Kato, S. Matsuda, T. Kamo, F. Nakajima, H. Kuroda, T. Narita, J. Phys. Chem. 85 (1981) 4099–4102.
[11] E. Xue, K. Seshan, J.R.H. Ross, Appl. Catal. B 11 (1996) 65–79.
[12] J. Després, M. Elsener, M. Koebel, O. Kröcher, B. Schnyder, A. Wokaun, Appl. Catal. B 50 (2004) 73–82.
[13] P.J. Schmitz, R.J. Kudla, A.R. Drews, A.E. Chen, C.K. Lowe-Ma, R.W. McCabe, W.F. Schneider 1, C.T. Goralski Jr., Appl. Catal. B 67 (2006) 246–256.
[14] L. Olsson, E. Fridell, J. Catal. 210 (2002) 340–353.
[15] M.M. Yung, E.M. Holmgreen, U.S. Ozkan, J. Catal. 247 (2007) 356–367.
[16] M.F. Irfan, J.H. Goo, S.D. Kim, Appl. Catal. B 78 (2008) 267–274.
[17] Q. Wang, S.Y. Park, J.S. Choi, J.S. Chung, Appl. Catal. B 79 (2008) 101–107.
[18] Q. Wang, S.Y. Park, J.S. Chung, Appl. Catal. B 85 (2008) 10–16.
[19] T. Naota, H. Takaya, S. Murahashi, Chem. Rev. 98 (1998) 2599–2660.
[20] S. Freni, G. Calogero, S. Cavallaro, J. Power Sources 87 (2000) 28–38.
[21] M.A. Vannice, R.L. Garten, J. Catal. 63 (1980) 255–260.
[22] S.R. Tennison, in: J.R. Jennings (Ed.), Catalyic Ammonia Synthesis, Plenum Press, New York, 1991, pp. 303–364.
[23] N. Li, C. Descorme, M. Besson, Appl. Catal. B 71 (2007) 262–270.
[24] D. Pham Minh, G. Aubert, P. Gallezot, M. Besson, Appl. Catal. B 73 (2007) 236–246.
[25] A. Pintar, J. Batista, T. Tišler, Appl. Catal. B 84 (2008) 30–41.
[26] T. Mitsui, K. Tsutsui, T. Matsui, R. Kikuchi, K. Eguchi, Appl. Catal. B 81 (2008) 56–63.
[27] R. Lanza, S.G. Järås, P. Canu, Appl. Catal. A 325 (2007) 57–67.
[28] R. Giles, N.W. Cant, M. Kögel, T. Turek, D.L. Trimm, Appl. Catal. B 25 (2000) L75–L81.
[29] G.C. Bond, R.R. Rajaram, R. Burch, Appl. Catal. 27 (1986) 379–391.
[30] S. Matsuda, A. Kato, Appl. Catal. 8 (1983) 149–165.
[31] L. Ji, J. Lin, H.C. Zeng, Chem. Mater. 13 (2001) 2403–2412.
[32] T. Chafik, A.M. Efstathiou, X.E. Verykios, J. Phys. Chem. B 101 (1997) 7968–7977.
[33] M.A. Debeila, N.J. Coville, M.S. Scurrell, G.R. Hearne, Appl. Catal. A 291 (2005) 98–115.
[34] K. Hadjiivanov, Catal. Rev. Sci. Eng. 42 (2000) 71–144.
[35] G. Ramis, G. Busca, V. Lorenzelli, P. Forzatti, Appl. Catal. 64 (1990) 243–257.
[36] K. Hadjiivanov, H. Knozinger, Phys. Chem. Chem. Phys. 2 (2000) 2803–2806.
[37] L.D. Li, F.X. Zhang, N.J. Guan, E. Schreier, M. Richter, Catal. Commun. 9 (2008) 1827–1832.
[38] E. Guglielminotti, F. Boccuzzi, J. Catal. 141 (1993) 486–493.
[39] L.D. Li, J.J. Yu, Z.P. Hao, Z.P. Xu, J. Phys. Chem. C 111 (2007) 10552–10559.
[40] Z. Liu, J.A. Anderson, J. Catal. 224 (2004) 18–27.